Volume 19 | Number 25 | 7 July 2017 | Pages 3373–3528

CrystEngComm

rsc.li/crystengcomm

ROYAL SOCIETY OF CHEMISTRY

HIGHLIGHT

Julia Y. Chan *et al.*

The proof is in the powder: revealing structural peculiarities in the $Yb_3Rh_4Sn_{13}$ structure type

CrystEngComm

HIGHLIGHT

View Article Online
View Journal | View Issue

Cite this: *CrystEngComm*, 2017, **19**, 3381

The proof is in the powder: revealing structural peculiarities in the $Yb_3Rh_4Sn_{13}$ structure type†

Iain W. H. Oswald,[a] Binod K. Rai,[ab] Gregory T. McCandless,[a] Emilia Morosan[ab] and Julia Y. Chan *[a]

Received 28th February 2017,
Accepted 18th April 2017

DOI: 10.1039/c7ce00419b

rsc.li/crystengcomm

Compounds adopting the $Yb_3Rh_4Sn_{13}$ structure type have drawn attention because of the revelation of exotic states such as heavy fermion behavior, superconductivity, charge density wave, and quantum critical behavior. The prototypical structure has historically been modeled with a primitive cubic space group, $Pm\bar{3}n$; however, structural studies have led to the realization of disordered atomic sites, requiring lower symmetry models. We will review the low symmetry models required to describe the structural distortions in the related $Yb_3Rh_4Sn_{13}$ structure type. In addition, we present the structure determination of a new analogue, $Lu_3Ir_4Ge_{13}$, which adopts a new structural model in $I4_1/amd$.

Introduction

Single crystal growth and structure determination are crucial to understanding the intrinsic properties of a new material.[1,2] This is especially the case in complex phases and/or when disorder is present, as small structural changes can have drastic effects on physical properties. For example, the low lattice thermal conductivity discovered in bulk stannides, such as $Gd_{117}Co_{56}Sn_{112}$ (ref. 3) and $Ln_{30}Ru_4Sn_{31}$ (Ln = Gd, Dy) (ref. 4), with complex structures (as determined through detailed structure elucidation) would not be possible without the growth of single crystals. Single crystals also allowed the discovery of the magnetic field-pulse memory effect and anisotropic magnetic and electrical properties in a 3-dimensional stannide $Tb_{30}Ru_{6.0}Sn_{29.5}$.[5] The $Yb_3Rh_4Sn_{13}$ structure type represents yet another class of material with a rich history of crystal chemistry due to the presence of disorder, which has led to a multitude of structural models to be reported.[6–10] As such, it is timely to review the structural details and modelling of this class of materials.

The $Yb_3Rh_4Sn_{13}$ structure type[6,11,12] and related variants have come under investigation in the last several years for both their magnetic and electrical properties as well as rich

[a] *University of Texas at Dallas, USA. E-mail: Julia.Chan@utdallas.edu*
[b] *Department of Physics and Astronomy, Rice University, 6100 Main Street, Houston, Texas 77005, USA*

† Electronic supplementary information (ESI) available. See DOI: 10.1039/c7ce00419b

Iain Oswald

Iain Oswald received his B.Sc. and M.Sc. in Chemistry in 2010 and 2013, respectively, from the University of North Texas. He is currently pursuing his PhD under the direction of Prof. Julia Y. Chan at the University of Texas at Dallas. His research interests include structural characterization of phase transition materials in magnetocalorics and optical materials, and elucidating structural disorder in complex gallides, germanides, and stannides using powder and single crystal X-ray diffraction and correlating physical properties. In addition, he has synthesized novel low dimensional materials to exploit their anisotropic electronic properties.

Binod Rai

Binod Rai received a M.S. degree in Physics from the University of Memphis in 2012. He is currently a Ph.D. candidate at Rice University, working in Professor Emilia Morosan's group. His research interests include Kondo systems, magnetism and superconductivity.

crystal chemistry.[6,7,9–20] Since their initial discovery by Remeika and co-workers in 1980,[11] over 100 compounds have been synthesized, highlighting the robustness of the structure type. Investigations of their electrical properties have revealed several exotic states, including superconductivity,[6,8,13,15–17,21–25] heavy electron behavior,[20,26–28] intermediate valence behavior,[28,29] charge density wave,[19,30–32] and giant magnetoresistance.[33] More recently, doping studies of $Yb_3(Rh_{1-x}T_x)Ge_{13}$ (T = Co, Ir) revealed a suppression of magnetic ordering with decreasing x that is concomitant with non-Fermi-liquid behavior and quantum critical behavior.[20]

Although many germanides and stannides of this family show a decrease in resistivity (metallic) upon cooling prior to becoming superconductors,[34] we have found that the compounds $Lu_3T_4Ge_{13}$ (T = Co, Rh, Os) and $Y_3T_4Ge_{13}$ (T = Ir, Rh, Os) show an increase in resistivity (semi-metal-like) instead. We found an empirical correlation between atomic site disorder, quantified by atomic displacement parameters, and the electrical properties of these materials, highlighting how crystallography can be used to help understand and predict physical properties.[17] In this review, we describe the crystal chemistry of the $Yb_3Rh_4Sn_{13}$ structure type and related lower symmetry structural variants. We will first highlight the discovery of compounds of this structure type and the general structural motifs, followed by the elucidation of disorder and structural distortions, and finally highlight more recently reported models describing new compounds and how they relate to the prototypical cubic structure.

Gregory McCandless

Gregory McCandless is an X-ray crystallographer in the Department of Chemistry and Biochemistry at the University of Texas at Dallas. During his PhD work at Louisiana State University, he was awarded the International Centre for Diffraction Data (ICDD) Ludo Frevel Crystallography Scholarship Award. His research focus is chemical crystallography at the interface of chemistry, physics, and engineering.

The $Yb_3Rh_4Sn_{13}$ structure type

The $Yb_3Rh_4Sn_{13}$ structure type was first reported in 1980 by Remeika and co-workers that included the compounds $A_3Rh_4Sn_{13}$ (A = La, Ce, Pr, Nd, Sm, Eu, Gd, Yb, Th, Ca and Sr).[11] This initial report of several stannide analogues provided only the cubic unit cell parameter ($a \sim 9.7$ Å) and the space group selection ($Pm\bar{3}n$). In subsequent months, the crystal structures of $Pr_3Rh_4Sn_{13}$ and $Yb_3Rh_4Sn_{13}$ were published, describing the atomic positions and thermal parameters.[6,35] Further studies expanded the list of compositions to include cobalt and iridium containing compounds, such as the series $A_3Ir_4Sn_{13}$ (A = La, Ce, Pr, Nd, Sm, Yb, Ca, Sr) and $A_3Co_4Sn_{13}$ (A = Yb, Ca).[12] This was followed by yet another report on the series A–Co–Sn, A–Ru–Sn, and A–Os–Sn (A = rare earth, Y).[36]

The unit cell of $Yb_3Rh_4Sn_{13}$ is shown in Fig. 1, and Table 1 contains the atomic positions. There are four atomic positions in the cell: Yb (Wyckoff position 6*d*), Rh (8*e*), Sn1 (2*a*) and Sn2 (24*k*) as provided in Table 1. The two crystallographically distinct Sn atoms (henceforth, referred to as Sn1 and Sn2, respectively) have quite different character based on bond lengths and atomic displacement parameters: the Sn1–

Emilia Morosan

Emilia Morosan is a Professor of Physics and Astronomy, Chemistry, and Materials Science and Nanoengineering at Rice University. She has been at Rice since 2007, following doctoral work at Iowa State University and a postdoc at Princeton University. Her research in condensed matter experiments is focused on itinerant magnetism, superconductivity, Kondo systems and quantum criticality. She uses different crystal growth methods (flux and vapor transport) as well as basic characterization techniques. Prof. Morosan received the NSF CAREER award, the PECASE award, and the Humboldt fellowship for experienced researchers and in 2014 was named a Moore Foundation EPiQS Investigator.

Julia Chan

Julia Chan is a Professor of Chemistry and Biochemistry at the University of Texas at Dallas. She received her PhD at UC Davis and was a National Research Council Postdoctoral fellow at NIST. Her research is focused on the crystal growth and characterization of highly correlated systems, magnetocalorics, and thermoelectrics. Prof. Chan received the NSF CAREER Award, American Crystallographic Association Margaret C. Etter Early Career Award, Alfred P. Sloan Research Fellowship, Iota Sigma Pi Agnes Fay Morgan Award, and the ACS Exxon Mobil Faculty Fellowship in Solid State Chemistry. She is currently serving as an associate editor of Science Advances.

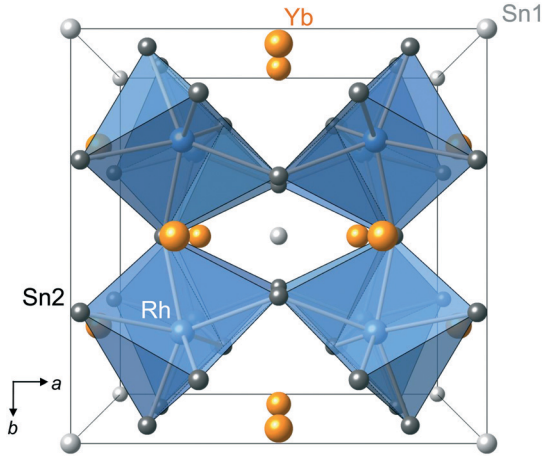

Fig. 1 Cubic unit cell of $Yb_3Rh_4Sn_{13}$ showing $Rh(Sn2)_6$ trigonal prisms.

Table 1 Atomic positions of $Yb_3Rh_4Sn_{13}$ in $Pm\bar{3}n$[6]

Atom	Wyckoff site	x	y	z
Yb	6*d*	$\frac{1}{4}$	$\frac{1}{2}$	0
Rh	8*e*	$\frac{1}{4}$	$\frac{1}{4}$	$\frac{1}{4}$
Sn1	2*a*	0	0	0
Sn2	24*k*	0	0.30570(4)	0.15333(3)

Sn2 interatomic distance of ~3.3 Å is long relative to that expected for a typical Sn–Sn bond (~2.8 Å),[37] indicating that any interactions between Sn1 and the surrounding Sn2 icosahedra are most likely weak.[35] Conversely, Rh–Sn2 and Yb–Sn2 have bond distances that are typical for covalent interactions.

The building blocks of the $Yb_3Rh_4Sn_{13}$ structure type are composed of $AuCu_3$-type $Sn1(Sn2)_{12}$ icosahedra and $Yb(Sn2)_{12}$ cuboctahedra, while Rh is surrounded by six Sn2 atoms creating trigonal prisms, as shown in Fig. 2. This formula is similar to that of the triple perovskite structure type, which has a general formula of $A'A''_3B_4X_{12}$, where A′, A″ and B are cations of different size, and X is an anion that links the building blocks together. As such, the $Yb_3Rh_4Sn_{13}$ structure-type formula is sometimes expressed as $(Sn1)Yb_3Rh_4(Sn2)_{12}$, emphasizing that Sn1 is more similar in ionic character to the rare earth element than Sn2.[6] The triple perovskite itself is related to the ubiquitous ABX_3 perovskite structure type, having the same structural building blocks, but with the octahedron

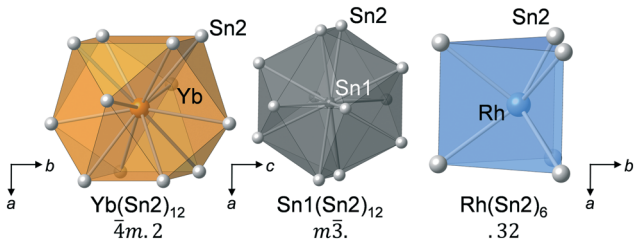

Fig. 2 Local environment and site symmetries of rare earth cuboctahedra (left), $Sn1(Sn2)_{12}$ icosahedra (center), and transition metal trigonal prisms (right) in $Yb_3Rh_4Sn_{13}$.

tilted relative to the undistorted parent. A formalism has been developed to relate $Yb_3Rh_4Sn_{13}$ to the perovskite structure type: Sn1 and the rare earth can be considered the "A"-site, Rh the "B"-site, and Sn2 the "X"-anionic site. Thus, this structure has been referred to as the "covalent counterpart" to the ionic ABX_3 perovskite structure. Fig. 3 shows a schematic relating the two structure types. Indeed, like the perovskite structure type, many combinations of elements exist for the $Yb_3Rh_4Sn_{13}$ structure type, allowing for tunable physical properties.

Soft and rigid bonding in the $Yb_3Rh_4Sn_{13}$ structure type

An important observation was made by Hodeau, Remeika, and co-workers regarding the thermal vibrations associated with the Sn2 atoms: the ellipsoids are highly anisotropic with B_{11}, B_{22}, and B_{33} of 0.00144, 0.00503, and 0.002211, respectively, and pointed towards the Sn1 atom at the center of the Sn2 icosahedron as illustrated in Fig. 4.[6] Miraglia and co-workers later showed that the disorder, as represented by the prolated thermal ellipsoid, is not dynamic – *i.e.* thermally driven – but has static, positional disorder along the Sn1–Sn2 bonds.[21] The thermal ellipsoid of Sn1 (B_{11} = 0.0040(1)) is also large in comparison to those of Yb (B_{11} = 0.00264(2) and B_{22} = 0.00213(3)) and Rh (B_{11} 0.00151(4)). Hence, the bonding within the $Sn1(Sn2)_{12}$ icosahedra was described as "soft", while the $Rh(Sn2)_6$ trigonal prisms and $Yb(Sn2)_{12}$ cuboctahedra bonding is "rigid". This is a consequence of the Sn1 and Sn2 atoms having different ionic character (deduced by bond distances) that varies from ionic to covalent: the Sn1 is more cationic, and the Sn2 more anionic. Similarly, large thermal parameters have since been observed in almost every compound of this structure type, making this "soft" and "rigid" bonding concept a general feature.

The elucidation of disorder

Several structural studies have been pursued due to the presence of crystallographic disorder of the anionic main group element (such as Ge or Sn) surrounding the cationic Sn/Ge and rare earth/alkaline earth atoms.[7,9,10,18,19,21,38,39] Even the earliest report of structure determinations noted structural distortions leading to lower symmetry space groups.[38] Structural investigations of $A_3Rh_4Sn_{13}$ (A = La, Ce, Pr, Nd, Sm, and Gd) using long exposure times revealed weak superstructure reflections (200 hours), suggesting a lower symmetry model is necessary to best describe the structure that accounts for these reflections.[38] Conversely, no indication of distortion was observed in the compounds $A_3Rh_4Sn_{13}$ where A = Eu, Yb, Ca, Sr, and Th. It was noted that the valency (either trivalent or divalent) appears to correlate with the distortion, but the size of the A atoms does not.[38] Superstructure reflections in $La_3Rh_4Sn_{13}$ precession images were indexed using a body-centered cubic cell roughly double the length of the primitive cubic cell, *i.e.* $a_{body} \approx 2a_{primitive}$. Reflection conditions correspond to the non-centrosymmetric space group $I2_13$,

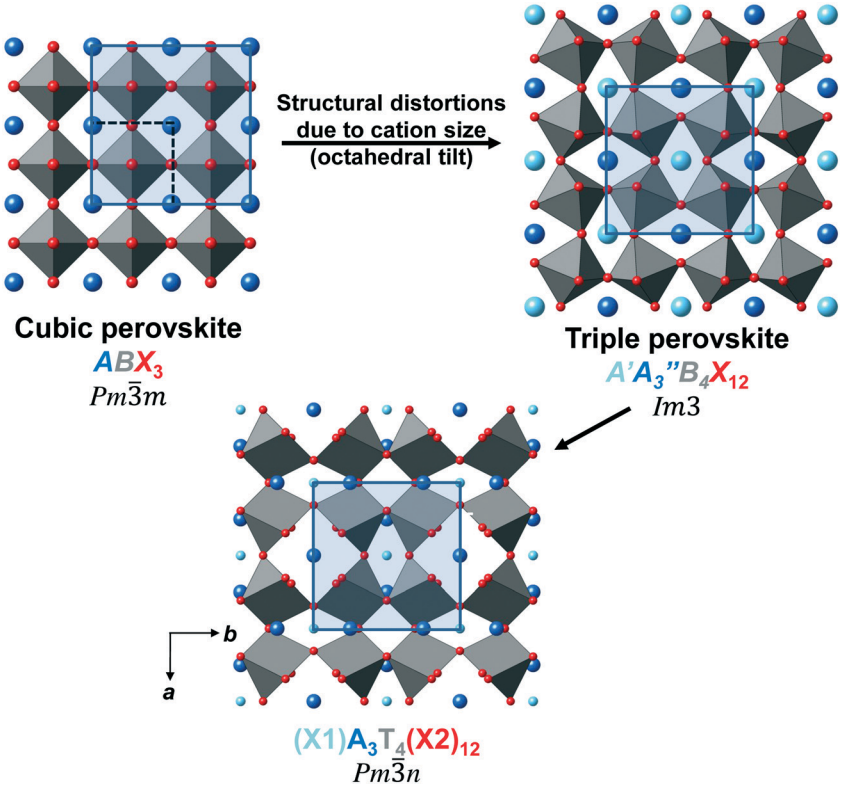

Fig. 3 Relationship between the cubic perovskite structure, the distorted triple perovskite, and the primitive cubic unit cell of the $(Sn1)Yb_3Rh_4(Sn2)_{13}$ structure type.

although it was noted that only one weak reflection (14 0 0) was present that violated the systematic absences of the 4_1 screw axis ($h \neq 4n$ for h 0 0). Thus, space group $I4_132$ could be considered if this reflection is disregarded.

Using the primitive cubic cell and body-centered supercell leads to subtle yet apparent differences: the $Sn1(Sn2)_{12}$ icosahedral cluster is distorted enough to break the local $m\bar{3}$ symmetry of the Sn1 site, lowering the overall symmetry of the cell and best modelled in the body centered supercell (Fig. 5). In the primitive cubic cell, Sn2 atoms are equidistant from Sn1, forming an icosahedron. In the body centered supercell model, the atomic positions of the Sn2 atoms are no longer constrained by symmetry, allowing them to be further or closer to the Sn1 in a distorted icosahedral arrangement. A more recently reported structure determination of the compound $La_3Rh_4Sn_{13}$ using synchrotron powder X-ray diffraction revealed a structure that was modeled in space group $I4_132$ with lattice parameter a = 19.492 Å, confirming the results from the prior report.[40]

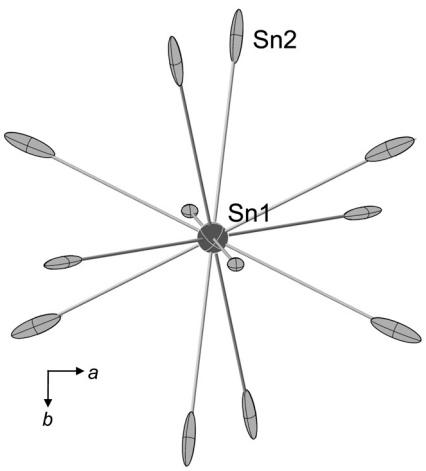

Fig. 4 Local environment of Sn1 surrounded by Sn2 in $Yb_3Rh_4Sn_{13}$. The large, elongated thermal ellipsoids of the Sn2 atoms are directed toward the Sn1 atom at the center of the icosahedron.

The expansion of structural models

Since the initial structural distortion was determined, many lower symmetry models have been reported.[7,9,10,19] Although the general structural building blocks are still present, the distortions can be subtly different (as evident by reflections in diffraction data), and should be represented with models reflecting the local structure. Described below are some examples, their structural models, and how they are related to the cubic archetypal $Yb_3Rh_4Sn_{13}$ structure type. Space groups, lattice constants, and volumes can be found in Table 2, while Fig. 6 shows the $X1(X2)_{12}$ polyhedra relative to the non-distorted icosahedra found in $Yb_3Rh_4Sn_{13}$ with the various X2 colors indicating those related by symmetry.

$Ca_3Pt_{4+x}Ge_{13-y}$ and $Yb_3Pt_4Ge_{13}$ were synthesized using high-pressure, high-temperature methods.[7] The former could be indexed using a body centered cubic cell with lattice

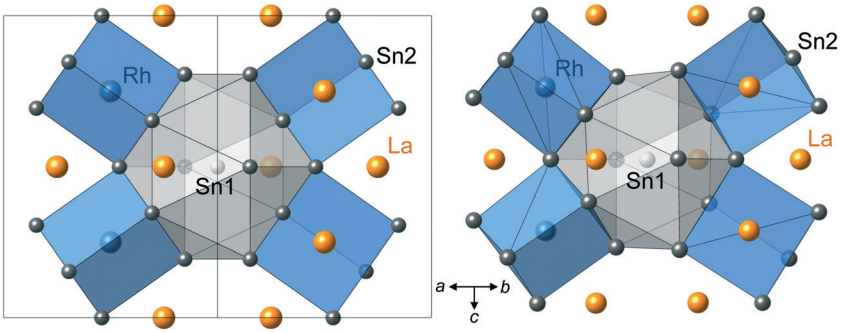

Fig. 5 Projections of $La_3Rh_4Sn_{13}$ $Sn1(Sn2)_{12}$ icosahedra and $Rh(Sn2)_6$ trigonal prisms in the undistorted primitive cubic (left) and distorted body centered cubic (right) structures along the [110] direction.

Table 2 Crystallographic details of selected compounds derived from the $Yb_3Rh_4Sn_{13}$ structure type

Compound	Space group	Lattice constants (Å)	Volume	Ref.
$Yb_3Rh_4Sn_{13}$	$Pm\bar{3}n$ (no. 223)	a = 9.676(1)	905.9(1)	6
$La_3Rh_4Sn_{13}$	$I4_132$ (no. 213)	a = 19.4918(4)	7405.52(4)	40
$Ca_3Pt_{4+x}Ge_{13-y}$	$I2_13$ (no. 199)	a = 18.0578(1)	5888.3(1)	7
$Yb_3Pt_4Ge_{13}$	$P4_2cm$ (no. 101)	a = 12.7479(1) c = 9.0009(1)	1462.7(1)	7
$Y_3Pt_4Ge_{13}$ (low T)	Cc (no. 9)	a = 12.8781(2) b = 12.8381(2) c = 9.1081(1) β = 89.954(2)°	1505.84(7)	10
$Y_3Pt_4Ge_{13}$ (high T)	$R3c$ (no. 161)	a = 12.7423(1) b = 15.6888(1)	2206.0(1)	9
$Th_3Ir_4Ge_{13}$	$Pm\bar{3}n$ (no. 223)	a = 9.0586(3)	743.33(13)	18
$U_3Ir_4Ge_{13}$	$R3c$ (no. 161)	a = 12.6329(1) c = 15.5505(1)	2149.26(5)	18
$Lu_3Ir_4Ge_{13}$	$I4_1/amd$ (no. 141)	a = 17.7674(11) c = 17.8229(13)	5626.3(8)	This work
$Ce_3Co_4Sn_{13}$ (298 K)	$Pm\bar{3}n$ (no. 223)	a = 9.6022(5)	885.34(8)	27
$Ce_3Co_4Sn_{13}$ (<160 K)	$I2_13$ (no. 199)	a = 19.1618(1)	7035.95(1)	19
$Sr_3Ir_4Sn_{13}$ (<152 K)	$I\bar{4}3d$ (no. 220)	a = 19.5947(3)	7523.43(9)	8

parameter a ~18.06 Å, which is similar to $La_3Rh_4Sn_{13}$. Space groups $I2_13$ and $I4_132$ were both evaluated; however, the intensities of the observed reflections were in better agreement with the calculated intensities from the structural model using $I2_13$ (Fig. 7). Still, some peculiarities remained: large displacement parameters for Ge1 (8*a* – the central site of the icosahedron) and Ge4 (24*c*) suggested partial occupancies, while another 8*a* atomic site required site mixing of Ge and Pt to obtain reasonable isotropic displacement parameters. These slight changes in occupation and site mixing result in the off-stoichiometry formula $Ca_3Pt_{4.1}Ge_{12.6}$. The distortions significantly affect bond lengths, with some Pt–Ge distances shortening by up to 5.2% from the sum of the atomic radii of the two elements. To accommodate this change, some Ge–Ge distances concomitantly increase, thereby changing the coordination number of the Ge at the center of the icosahedra from 12 to 10.

$Yb_3Pt_4Ge_{13}$, like $Ca_3Pt_{4.1}Ge_{12.6}$, can be roughly indexed to the primitive cubic cell with lattice constant a = 9.0045 Å. In this case, high-resolution synchrotron radiation proved to be an invaluable technique as the peak splitting of some reflections (such as the (4 0 0) shown in Fig. 8, left) is subtle enough to be hidden if overlapping reflections are not resolved. This distortion leads to a tetragonal cell with space group $P4_2cm$ and dimensions a = 12.7479(1) Å and c = 9.0009(1) Å (powder diffraction data and fitting shown in Fig. 8, right).

$Y_3Pt_4Ge_{13}$: low temperature structure

Similar to $Ca_3Pt_{4+x}Ge_{13-y}$ and $Yb_3Pt_4Ge_{13}$, $Y_3Pt_4Ge_{13}$ was synthesized at high pressure: the sample was pressed at 8 GPa and heated at 850 °C and annealed for two hours.[9] Synchrotron X-ray diffraction data revealed weak, unindexed reflections similar to $Ca_3Pt_{4+x}Ge_{13-y}$ and $Yb_3Pt_4Ge_{13}$. In addition, the cubic reflection (2 0 0) was split into two parts, indicating the possibility of a distorted tetragonal structure. Further analysis led to the selection of the lower symmetry monoclinic space group Cc, which is the lowest symmetry model for any of the distorted variants. $Y_3Pt_4Ge_{13}$ is one of the few examples of a non-centrosymmetric superconductor (T_c = 7 K). The series of compounds $A_3Pt_4Ge_{13}$ (A = Pr, Sm, Gd, Tb, and Tm) have the same structure at room temperature, indicating that within this series the distortions are general,

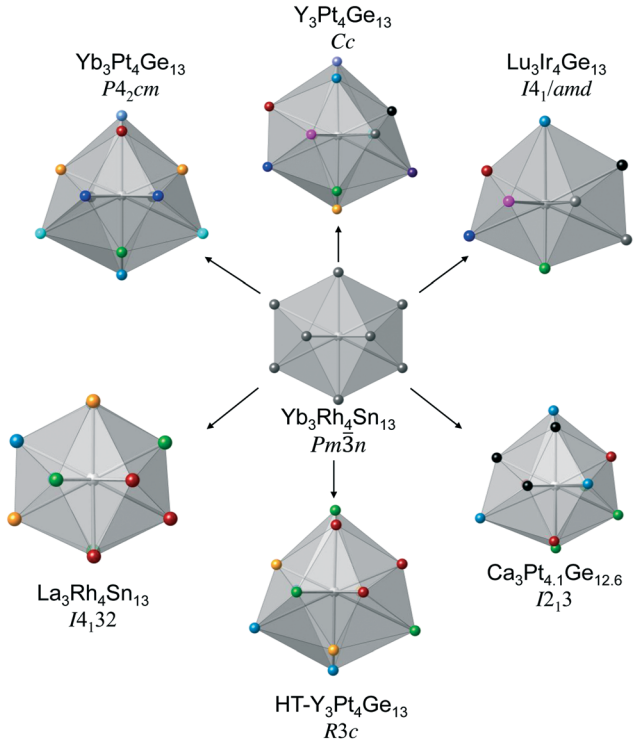

Fig. 6 A schematic showing the polyhedral representation of the local $X1(X2)_{12}$ (X = Ge or Sn) distorted icosahedra derived from $Yb_3Rh_4Sn_{13}$. The colors indicate the X2 atoms that are related by symmetry.

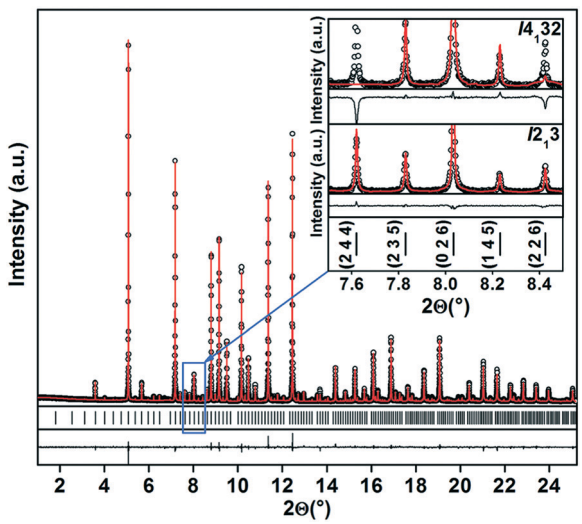

Fig. 7 Powder diffraction pattern of $Ca_3Pt_{4.1}Ge_{12.6}$. The inset shows indexing using space groups $I4_132$ (top) and $I2_13$ (bottom). Reproduced from ref. 7 with permission from The Royal Society of Chemistry.

where the rare earth valence is 3+ and the transition metal is Pt.

$Y_3Pt_4Ge_{13}$: high temperature structure

Differential scanning calorimetry (DSC) showed a first order phase transition at around 350 K for $Y_3Pt_4Ge_{13}$, indicating that a structural transformation could be occurring at this temperature,[10] at which point synchrotron diffraction experiments were conducted at 480 K to confirm. Once again, the majority of reflections could be indexed using space group $Pm\bar{3}n$ ($a \sim 9.03$ Å). However, the (h h h) reflections were split, leading to the noncentrosymmetric rhombohedral space group $R3c$ with fully occupied sites. It was noted that this reduction of symmetry arises strictly from the Ge-atomic sites, rather than Y or Pt.

$A_3Ir_4Ge_{13}$ (A = Yb, Lu): low carrier Kondo semimetals

We recently investigated thermodynamic, transport and optical properties on single crystals of $(Yb_{1-x}Lu_x)_3Ir_4Ge_{13}$ (x = 0, 0.2, 0.4, 0.5, 0.55, 0.6, 0.7, 0.8, 0.9, and 1.0) grown using the self-flux method.[41] A coexistence of the low-carrier density, Kondo effect, antiferromagnetic order, and quantum fluctuations near a quantum critical point establishes (Yb, $Lu)_3Ir_4Ge_{13}$ as a unique compound within the $A_3T_4X_{13}$ family.[42] These phases, like those mentioned previously, can be indexed based on the primitive cubic cell, but again have weak reflections in powder X-ray diffraction data as indicated by stars in the topmost pattern in Fig. 9. Furthermore, all analogues except x = 0.2 have peak splitting of the reflections corresponding to the primitive cubic cell, indicating an additional lowering of symmetry. The weak reflections present in powder diffraction data were also observed in single crystal X-ray diffraction precession images, as shown in Fig. 10. Both single crystal and powder X-ray diffraction data could be modelled using the tetragonal space group $I4_1/amd$ with lattice constants a = 17.7674(11) Å and c = 17.8229(13) Å. The small elongation of the c-axis breaks the cubic symmetry which in turn splits many of the major reflections corresponding to the cubic archetype. A notable feature in the structure is positional disorder of the Ge1 atom within the icosahedron. This atomic site is split (labeled Ge1A and Ge1B) in a ratio of roughly 92% and 8%, respectively. The crystallographic details can be found in Table 3, while atomic positions and thermal parameters are located in Table 4.

$A_3T_4Ge_{13}$ (A = Lu, Y; T = Co, Rh, Ir, Os)

We have also reported on a series of germanides that were synthesized using the self-flux method with semimetal-like electrical resistivity prior to becoming superconductors at low temperature ($T_c < 2$ K).[17,41] This unusual increase in resistivity coincides with a decrease in charge carrier density upon cooling in the normal state even though band structure calculations suggested a metallic ground state. These seemingly conflicting results were empirically resolved when we found a correlation between the disorder in the crystal structure and the electrical property of the materials. The amount of disorder was quantified by the following equation:

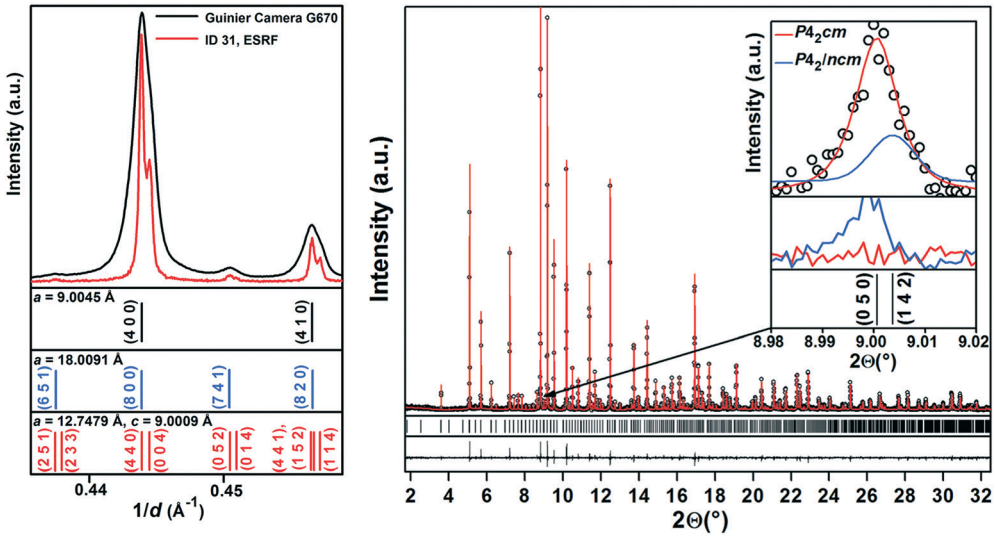

Fig. 8 Left: selected reflections showing clear peak splitting using high resolution synchrotron data *versus* a standard in-house detector. Right: powder diffraction pattern of $Yb_3Pt_4Ge_{13}$. Experimental (black points) and calculated (red line). Reproduced from ref. 7 with permission from The Royal Society of Chemistry.

$$\text{ADP ratio} = U_{\text{eq}(2a)}/U_{\text{eq}(T)}$$

where $U_{\text{eq}(2a)}$ is the atomic displacement parameter (ADP) for the Sn1 or Ge1 atom located at Wyckoff site 2*a*, and $U_{\text{eq}(T)}$ is the ADP for the transition metal element located at Wyckoff site 8*e*. In general, compounds with lower ADP ratios (less disorder) were more metallic, while those with a larger ADP ratio (more disorder) were more semiconductor-like. For instance, the semiconductor-like compounds $Lu_3Os_4Ge_{13}$ and $Y_3Ir_4Ge_{13}$ have ADP ratios of 6.7 and 13, respectively, while the metallic compounds $Yb_3Co_4Ge_{13}$ and $La_3Co_4Sn_{13}$ have ADP ratios of 0.94 and 1.6, respectively. This is a general feature for this class of material and can be used as a "rule of thumb" when predicting the electrical character of a compound of this type, similar to other rules developed for thermoelectric material development using ADPs.[43]

Temperature dependent structural distortions

Thus far, the structural studies of the compounds reviewed have been reported at room temperature or elevated temperatures. On the other hand, some compounds have recently been reported to undergo structural changes at lower temperatures – usually from the cubic primitive cell to a lower symmetry supercell. In some cases, features in physical property measurements, such as magnetization or resistivity, hint at the possibility of a structural transformation, although low temperature structural studies have demonstrated conflicting results regarding this.[8,19,27,30,32]

For instance, the superconductors $Ca_3Ir_4Sn_{13}$ (T_c = 7 K) and $Sr_3Ir_4Sn_{13}$ (T_c = 5 K) have garnered interest due to the presence of an anomaly in the electrical resistivity and magnetic susceptibility at 33 K and 147 K, respectively.[8] This feature was ascribed to a structural phase transition going from the primitive cubic cell to a supercell similar to the $La_3Rh_4Sn_{13}$ superstructure (space group $I4_132$) with $a \sim 19.5$ Å upon cooling (T = 147 K for $Sr_3Ir_4Sn_{13}$ and T = 33 K for $Ca_3Ir_4Sn_{13}$). The structural change was attributed to a charge density wave transition of the conduction electrons that could be modified by chemical or physical pressure. However, unlike the previously reported phases modeled in $I4_132$ or $I2_13$, this structure was best modeled using space group $I\bar{4}3d$. The major change was due to a distortion in the $Sn1(Sn2)_{12}$ icosahedra that coincides with tilting of 75% of the Ir trigonal prisms, while those with their axis oriented along the (111) direction remain unchanged. The transition temperature can be tuned by doping Ca on the Sr position, and eventually eliminated completely by application of hydrostatic pressure.

$Ce_3Co_4Sn_{13}$ is a heavy fermion compound that has also recently become the subject of studies due to an anomaly in resistivity at 160 K.[19,30,44,45] Initial low temperature structural studies did not reveal evidence of a transformation;[27] however, recent experiments have indeed observed weak reflections forbidden by the primitive cubic symmetry that can be indexed in a supercell and best modelled in space group $I2_13$.[19] This structural distortion may have a pronounced impact on the electrical properties of the material. Specific heat, Seebeck coefficient, thermal conductivity and NMR measurements suggest charge density wave formation occurring at the feature in resistivity.[30] However, exactly how the structural transformation is related to the CDW is still debated.

Conclusions and outlook

The importance of determining the best representation of the structure of a compound is perhaps most evident in the study

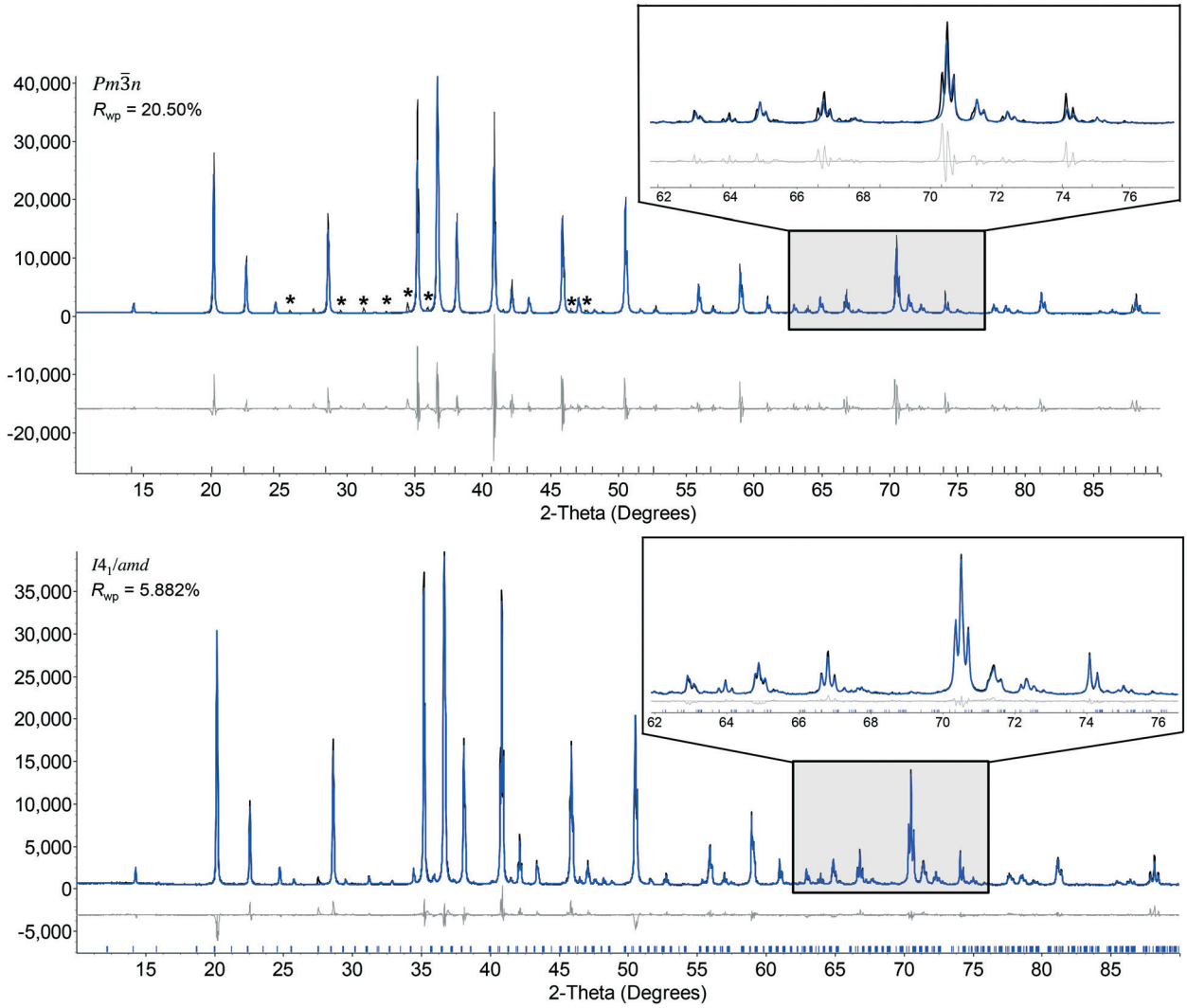

Fig. 9 Experimental (black line) and calculated (blue line) powder diffraction pattern of $Lu_3Ir_4Ge_{13}$ using space groups $Pm\bar{3}n$ (top) and $I4_1/amd$ (bottom). Stars indicate unindexed reflections.

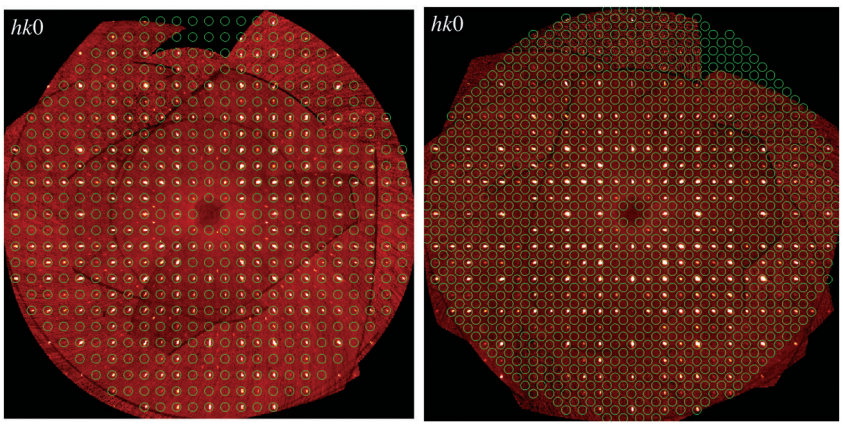

Fig. 10 Left: single crystal diffraction precession image of $Lu_3Ir_4Ge_{13}$ along the *hk*0 with $Pm\bar{3}n$ indexing showing weak, unindexed periodic reflections. Right: single crystal diffraction precession image of $Lu_3Ir_4Ge_{13}$ with $I4_1/amd$ indexing showing all reflections being indexed.

of physical properties, such as magnetism, electrical character, and transport. A wide array of phenomena have been observed in this family, including superconductivity,[8,9,11,17,36] charge density wave,[30,32,39] intermediate valence,[20] the Kondo

Table 3 $Lu_3Ir_4Ge_{13}$ crystallographic parameters

Formula	$Lu_3Ir_4Ge_{13}$
Crystal system	Tetragonal
Space group	$I4_1/amd$
a (Å)	17.764(3)
c (Å)	17.822(4)
V (Å^3)	5624(2)
Z	16
Crystal dimensions (mm^3)	0.10 × 0.08 × 0.05
θ range (°)	3.2–30.5
μ (mm^{-1})	85.79
Temperature (K)	298(2)
Measured reflections	75 394
Independent reflections	2294
Reflections with $I > 2\sigma(I)$	1671
R_{int}	0.077
R_1 $(F)^a$	0.039
wR_2 ^{b}	0.109
Parameters	107
Restraints	0
Extinction coefficient	0.000052(3)
Goodness-of-fit on F^2	1.15

^{a} $R_1 = \sum||F_o| - |F_c||/\sum|F_o|$. ^{b} $wR_2 = [\sum[w(F_o^2 - F_c^2)^2]/\sum[w(F_o^2)^2]]^{1/2}$.

effect,[46] quantum criticality,[20,47,48] and giant magnetoresistance.[33] Accounting for and elucidation of the structural details can serve as a tool to shed insights into the physical properties and possible applications. For instance, previous reports have considered this structure type to be a potentially useful thermoelectric material due to its somewhat complex crystal structure and the presence of disorder, which can help lower thermal conductivity.[49] Doping studies on $Yb_3Co_{4-x}Ru_xSn_{13}$ (x = 0, 0.38) revealed a sign change in the thermopower at approximately 150 K, highlighting the tunability of properties by doping.[14]

Superconductivity is also sensitive to the structural nature of a material. Early on, it was found that many compounds exhibit superconductivity with T_c values typically less than 8 K, while others order magnetically.[12] For instance, $Yb_3Rh_4Sn_{13}$ is a conventional BCS superconductor with T_c ~8.6 K. Although this compound has an inversion center (like most other superconductors), some compounds in this family, such as $Y_3Pt_4Ge_{13}$ (space group Cc), lack an inversion center due to the structural distortions and yet become superconductors at low temperature (T_c = 4.5 K).[9] This can lead to novel and complex electronic states due in part to changes in spin degeneracy resulting in mixing of spin-singlet and triplet pairing states. The appearance of a charge density wave (CDW) at low temperatures in $Sr_3Ir_4Sn_{13}$ and $Ce_3Co_4Sn_{13}$ was surprising considering the three-dimensional nature of the materials. A CDW is typically found in lower dimensional materials such as Cu_xTiSe_2,[50] the transition-metal dichalcogenides,[51] and the cuprate superconductors.[52–54] For $Sr_3Ir_4Sn_{13}$, modulated satellite peaks observed in X-ray scattering below 147 K indicate that a CDW exists in the (1 1 0) plane, which was corroborated by changes in bond distances between Sn1 and Sn2 using extended X-ray absorption fine structure.[32]

Finally, new theories surrounding topological materials often require specific crystalline symmetries to be present in a material.[55–57] These include topological insulators,[58] which are insulating in the bulk, but have protected conductive states on the surface, and Dirac and Weyl semimetals,[59–62] each of which have their own unique properties arising from the electronic structure of the material.[56] In particular, Weyl fermions, which are chiral,[63] require certain symmetry elements within the crystal lattice, thereby limiting the possible number of space groups which can host them. Interestingly, space groups $I4_132$ and $I2_13$, which the compounds $La_3Rh_4Sn_{13}$ and $Ce_3Co_4Sn_{13}$ adopt, respectively, can theoretically host these Weyl fermions.[19]

In this review, we described the structural models derived from the $Yb_3Rh_4Sn_{13}$ structure type and present the structural details of $Lu_3Ir_4Ge_{13}$, a new distorted variant modeled in space group $I4_1/amd$. Materials new and old are being investigated with regard to their structural models, especially

Table 4 $Lu_3Ir_4Ge_{13}$ atomic positions and thermal parameters

Atom	x	y	z	U_{iso}^*/U_{eq} ^{a} (Å^2)	Occupancy (<1)
Lu1	0.5000	0.37512 (4)	0.00090 (4)	0.01787 (17)	
Lu2	0.25127 (2)	0.49873 (2)	0.1250	0.01803 (17)	
Lu3	0.0000	0.37479 (4)	0.00139 (4)	0.01794 (16)	
Ir1	0.12521 (2)	0.37489 (2)	0.12510 (2)	0.01447 (16)	
Ir2	0.37493 (2)	0.37507 (2)	0.1250	0.01462 (17)	
Ir3	0.12524 (2)	0.62476 (2)	0.1250	0.01441 (17)	
Ge1A	0.25101 (9)	0.7500	0.00572 (9)	0.0188 (4)	0.921 (4)
Ge1B	0.2560 (11)	0.7500	−0.0512 (12)	0.0188 (4)	0.079 (4)
Ge2	0.0000	0.32683 (9)	0.16875 (8)	0.0163 (3)	
Ge3	0.25016 (6)	0.32921 (6)	0.17106 (7)	0.0187 (2)	
Ge4	0.17331 (7)	0.41701 (7)	0.00032 (6)	0.0206 (3)	
Ge5	0.0000	0.66070 (9)	0.17652 (9)	0.0197 (3)	
Ge6	0.12683 (10)	0.2500	0.06517 (10)	0.0232 (4)	
Ge7	0.31496 (7)	0.38480 (8)	0.00042 (7)	0.0263 (3)	
Ge8	0.06910 (7)	0.50008 (6)	0.10763 (8)	0.0268 (3)	
Ge9	0.5000	0.35237 (13)	0.18191 (11)	0.0356 (5)	

^{a} U_{eq} is defined as one-third of the trace of the orthogonalized U_{ij} tensor.

concerning those with exotic physical properties. The general deformation of the structure from the cubic archetype is due to distortions in the $Sn1(Sn2)_{12}$ icosahedra. These small, but measurable, changes have required the development of completely new models with different degrees of symmetry. Using single crystal X-ray diffraction and powder X-ray diffraction as complementary techniques can help immensely when determining the details of the structures. As Robert S. Roth once wrote, "When indexing a pattern, account for *every* peak."[64]

Acknowledgements

The work at Rice University was supported by the Welch Foundation and AFOSR MURI. J. Y. C. acknowledges NSF-DMR1358975.

Notes and references

1 W. A. Phelan, M. C. Menard, M. J. Kangas, G. T. McCandless, B. L. Drake and J. Y. Chan, *Chem. Mater.*, 2012, **24**, 409–420.
2 D. C. Schmitt, B. L. Drake, G. T. McCandless and J. Y. Chan, *Acc. Chem. Res.*, 2015, **48**, 612–618.
3 D. C. Schmitt, N. Haldolaarachchige, Y. Xiong, D. P. Young, R. Jin and J. Y. Chan, *J. Am. Chem. Soc.*, 2012, **134**, 5965–5973.
4 D. C. Schmitt, N. Haldolaarachchige, J. Prestigiacomo, A. Karki, D. P. Young, S. Stadler, R. Jin and J. Y. Chan, *J. Am. Chem. Soc.*, 2013, **135**, 2748–2758.
5 D. C. Schmitt, J. C. Prestigiacomo, P. W. Adams, D. P. Young, S. Stadler and J. Y. Chan, *Appl. Phys. Lett.*, 2013, **103**, 082403.
6 J. L. Hodeau, J. Chenavas, M. Marezio and J. P. Remeika, *Solid State Commun.*, 1980, **36**, 839–845.
7 R. Gumeniuk, L. Akselrud, K. O. Kvashnina, W. Schnelle, A. A. Tsirlin, C. Curfs, H. Rosner, M. Schöneich, U. Burkhardt, U. Schwarz, Y. Grin and A. Leithe-Jasper, *Dalton Trans.*, 2012, **41**, 6299–6309.
8 L. E. Klintberg, S. K. Goh, P. L. Alireza, P. J. Saines, D. A. Tompsett, P. W. Logg, J. Yang, B. Chen, K. Yoshimura and F. M. Grosche, *Phys. Rev. Lett.*, 2012, **109**, 237008.
9 R. Gumeniuk, M. Nicklas, L. Akselrud, W. Schnelle, U. Schwarz, A. A. Tsirlin, A. Leithe-Jasper and Y. Grin, *Phys. Rev. B: Condens. Matter Mater. Phys.*, 2013, **87**, 224502.
10 R. Gumeniuk, M. Schoneich, K. O. Kvashnina, L. Akselrud, A. A. Tsirlin, M. Nicklas, W. Schnelle, O. Janson, Q. Zheng, C. Curfs, U. Burkhardt, U. Schwarz and A. Leithe-Jasper, *Dalton Trans.*, 2015, **44**, 5638–5651.
11 J. P. Remeika, G. P. Espinosa, A. S. Cooper, H. Barz, J. M. Rowell, D. B. McWhan, J. M. Vandenberg, D. E. Moncton, Z. Fisk, L. D. Woolf, H. C. Hamaker, M. B. Maple, G. Shirane and W. Thomlinson, *Solid State Commun.*, 1980, **34**, 923–926.
12 A. S. Cooper, *Mater. Res. Bull.*, 1980, **15**, 799–805.
13 G. P. Espinosa, A. S. Cooper, H. Barz and J. P. Remeika, *Mater. Res. Bull.*, 1980, **15**, 1635–1641.
14 D. C. Schmitt, N. Haldolaarachchige, D. P. Young, R. Jin and J. Y. Chan, *Z. Anorg. Allg. Chem.*, 2011, **637**, 2046–2051.
15 S. Y. Zhou, H. Zhang, X. C. Hong, B. Y. Pan, X. Qiu, W. N. Dong, X. L. Li and S. Y. Li, *Phys. Rev. B: Condens. Matter Mater. Phys.*, 2012, **86**, 064504.
16 D. A. Tompsett, *Phys. Rev. B: Condens. Matter Mater. Phys.*, 2014, **89**, 075117.
17 B. K. Rai, I. W. H. Oswald, J. K. Wang, G. T. McCandless, J. Y. Chan and E. Morosan, *Chem. Mater.*, 2015, **27**, 2488–2494.
18 R. Gumeniuk, K. O. Kvashnina, W. Schnelle, A. Leithe-Jasper and Y. Grin, *Phys. Rev. B: Condens. Matter Mater. Phys.*, 2015, **91**, 094110.
19 Y. Otomo, K. Iwasa, K. Suyama, K. Tomiyasu, H. Sagayama, R. Sagayama, H. Nakao, R. Kumai and Y. Murakami, *Phys. Rev. B*, 2016, **94**, 075109.
20 B. K. Rai, I. W. H. Oswald, J. Y. Chan and E. Morosan, *Phys. Rev. B*, 2016, **93**, 035101.
21 S. Miraglia, J. L. Hodeau, M. Marezio, C. Laviron, M. Ghedira and G. P. Espinosa, *J. Solid State Chem.*, 1986, **63**, 358–368.
22 M. Ya, A. Grytsiv, P. Rogl, C. Dusek, A. Galatanu, E. Idl, H. Michor, E. Bauer, C. Godart, D. Kaczorowski, L. Romaka and O. Bodak, *J. Phys.: Condens. Matter*, 2001, **13**, 7391.
23 J. Yang, B. Chen, C. Michioka and K. Yoshimura, *J. Phys. Soc. Jpn.*, 2010, **79**, 113705.
24 A. Ślebarski, M. Fijałkowski, M. M. Maśka, M. Mierzejewski, B. D. White and M. B. Maple, *Phys. Rev. B: Condens. Matter Mater. Phys.*, 2014, **89**, 125111.
25 C. V. Tomy, G. Balakrishnan and D. M. Paul, *Phys. Rev. B: Condens. Matter Mater. Phys.*, 1997, **56**, 8346–8350.
26 K. Ghosh, S. Ramakrishnan, S. K. Dhar, S. K. Malik, G. Chandra, V. K. Pecharsky, K. A. Gschneidner, Z. Hu and W. B. Yelon, *Phys. Rev. B: Condens. Matter Mater. Phys.*, 1995, **52**, 7267–7277.
27 E. Lyle Thomas, H.-O. Lee, A. N. Bankston, S. MaQuilon, P. Klavins, M. Moldovan, D. P. Young, Z. Fisk and J. Y. Chan, *J. Solid State Chem.*, 2006, **179**, 1642–1649.
28 H. Sato, T. Fukuhara, S. Iwakawa, Y. Aoki, I. Sakamoto, S. Takayanagi and N. Wada, *Phys. B*, 1993, **186**, 630–632.
29 B. K. Rai and E. Morosan, *APL Mater.*, 2015, **3**, 041511.
30 C. S. Lue, H. F. Liu, S. L. Hsu, M. W. Chu, H. Y. Liao and Y. K. Kuo, *Phys. Rev. B: Condens. Matter Mater. Phys.*, 2012, **85**, 205120.
31 A. F. Fang, X. B. Wang, P. Zheng and N. L. Wang, *Phys. Rev. B: Condens. Matter Mater. Phys.*, 2014, **90**, 035115.
32 H. T. Wang, M. K. Srivastava, C. C. Wu, S. H. Hsieh, Y. F. Wang, Y. C. Shao, Y. H. Liang, C. H. Du, J. W. Chiou, C. M. Cheng, J. L. Chen, C. W. Pao, J. F. Lee, C. N. Kuo, C. S. Lue, M. K. Wu and W. F. Pong, *Sci. Rep.*, 2017, **7**, 40886.
33 H. S. Nair, S. K. Ghosh, R. K. Kumar and A. M. Strydom, *J. Appl. Phys.*, 2016, **119**, 123901.
34 P. Neha, P. Srivastava, R. Jha, Shruti, V. P. S. Awana and S. Patnaik, *J. Alloys Compd.*, 2016, **665**, 333–338.
35 J. M. Vandenberg, *Mater. Res. Bull.*, 1980, **15**, 835–847.
36 G. P. Espinosa, A. S. Cooper and H. Barz, *Mater. Res. Bull.*, 1982, **17**, 963–969.

37 J. Emsley, *The Elements*, Oxford University Press, New York, 1998.
38 J. L. Hodeau, M. Marezio, J. P. Remeika and C. H. Chen, *Solid State Commun.*, 1982, **42**, 97–102.
39 C. N. Kuo, H. F. Liu, C. S. Lue, L. M. Wang, C. C. Chen and Y. K. Kuo, *Phys. Rev. B: Condens. Matter Mater. Phys.*, 2014, **89**, 094520.
40 P. Bordet, D. E. Cox, G. P. Espinosa, J. L. Hodeau and M. Marezio, *Solid State Commun.*, 1991, **78**, 359–366.
41 P. C. Canfield and Z. Fisk, *Philos. Mag. B*, 1992, **65**, 1117–1123.
42 B. K. Rai, I. W. H. Oswald, W. Ban, C.-L. Huang, S. Dzsaber, J. Y. Chan, N. L. Wang, S. Paschen, Q. Si and E. Morosan, Low-carrier-density and non-Fermi-liquid behavior in the Kondo system $Yb_3Ir_4Ge_{13}$, Manuscript in preparation.
43 B. C. Sales, D. G. Mandrus and B. C. Chakoumakos, in *Semiconductors and Semimetals*, ed. M. T. Terry, Elsevier, 2001, vol. 70, pp. 1–36.
44 A. Ślebarski and J. Goraus, *Phys. Rev. B: Condens. Matter Mater. Phys.*, 2013, **88**, 155122.
45 A. Ślebarski, J. Goraus and P. Witas, *Phys. Rev. B: Condens. Matter Mater. Phys.*, 2015, **92**, 155136.
46 C. L. Yang, X. Wang, X. Zhang, D. S. Wu, M. Liu, P. Zheng, J. Y. Yao, Z. Z. Li, Y. F. Yang, Y. G. Shi, J. L. Luo and N. L. Wang, *Phys. Rev. B: Condens. Matter Mater. Phys.*, 2015, **91**, 075120.
47 S. K. Goh, D. A. Tompsett, P. J. Saines, H. C. Chang, T. Matsumoto, M. Imai, K. Yoshimura and F. M. Grosche, *Phys. Rev. Lett.*, 2015, **114**, 097002.
48 P. K. Biswas, Z. Guguchia, R. Khasanov, M. Chinotti, L. Li, K. Wang, C. Petrovic and E. Morenzoni, *Phys. Rev. B: Condens. Matter Mater. Phys.*, 2015, **92**, 195122.
49 G. J. Snyder and E. S. Toberer, *Nat. Mater.*, 2008, **7**, 105–114.
50 E. Morosan, H. W. Zandbergen, B. S. Dennis, J. W. G. Bos, Y. Onose, T. Klimczuk, A. P. Ramirez, N. P. Ong and R. J. Cava, *Nat. Phys.*, 2006, **2**, 544–550.
51 J. A. Wilson, F. J. Di Salvo and S. Mahajan, *Phys. Rev. Lett.*, 1974, **32**, 882–885.
52 J. L. Hodeau, M. Marezio, C. Roucau, R. Ayroles, A. Meerschaut, J. Rouxel and P. Monceau, *J. Phys. C: Solid State Phys.*, 1978, **11**, 4117.
53 D. H. Torchinsky, F. Mahmood, A. T. Bollinger, I. Božović and N. Gedik, *Nat. Mater.*, 2013, **12**, 387–391.
54 D. A. Zocco, J. J. Hamlin, K. Grube, J. H. Chu, H. H. Kuo, I. R. Fisher and M. B. Maple, *Phys. Rev. B: Condens. Matter Mater. Phys.*, 2015, **91**, 205114.
55 X. Wan, A. M. Turner, A. Vishwanath and S. Y. Savrasov, *Phys. Rev. B: Condens. Matter Mater. Phys.*, 2011, **83**, 205101.
56 S.-Y. Xu, I. Belopolski, N. Alidoust, M. Neupane, G. Bian, C. Zhang, R. Sankar, G. Chang, Z. Yuan, C.-C. Lee, S.-M. Huang, H. Zheng, J. Ma, D. S. Sanchez, B. Wang, A. Bansil, F. Chou, P. P. Shibayev, H. Lin, S. Jia and M. Z. Hasan, *Science*, 2015, **349**, 613.
57 H. Watanabe, H. C. Po, M. P. Zaletel and A. Vishwanath, *Phys. Rev. Lett.*, 2016, **117**, 096404.
58 X.-L. Qi and S.-C. Zhang, *Rev. Mod. Phys.*, 2011, **83**, 1057–1110.
59 Z. Wang, Y. Sun, X.-Q. Chen, C. Franchini, G. Xu, H. Weng, X. Dai and Z. Fang, *Phys. Rev. B: Condens. Matter Mater. Phys.*, 2012, **85**, 195320.
60 Z. K. Liu, J. Jiang, B. Zhou, Z. J. Wang, Y. Zhang, H. M. Weng, D. Prabhakaran, S. K. Mo, H. Peng, P. Dudin, T. Kim, M. Hoesch, Z. Fang, X. Dai, Z. X. Shen, D. L. Feng, Z. Hussain and Y. L. Chen, *Nat. Mater.*, 2014, **13**, 677–681.
61 S. M. Young and C. L. Kane, *Phys. Rev. Lett.*, 2015, **115**, 126803.
62 Z. Gao, M. Hua, H. Zhang and X. Zhang, *Phys. Rev. B*, 2016, **93**, 205109.
63 L. Lu, Z. Wang, D. Ye, L. Ran, L. Fu, J. D. Joannopoulos and M. Soljačić, *Science*, 2015, **349**, 622.
64 R. S. Roth and J. Y. Chan, National Institute of Standards & Technology, private communication, 1999.